Electronic Supplementary Material (ESI) for Journal of Materials Chemistry A.
This journal is © The Royal Society of Chemistry 2022

Supplementary material

Biaxially oriented silica-polypropylene nanocomposites for HVDC film capacitors: Morphology-dielectric property relationships, and critical evaluation of the current progress and limitations

Ilkka Rytöluoto[a], Minna Niittymäki[b], Paolo Seri[c], Hadi Naderiallaf[c], Kari Lahti[b], Eetta Saarimäki[a], Timo Flyktman[a], & Mika Paajanen[a]

[a] VTT Technical Research Centre of Finland, Tampere, Finland.

[b] Laboratory of Electrical Engineering, Tampere University, Tampere, Finland.

[c] Electrical, Electronic and Information Engineering "Guglielmo Marconi" Dept., University of Bologna, Bologna, Italy.

Morphological analysis

Quantitative silica diameter, dispersion and distribution analysis was performed from several SEM micrographs by using ImageJ and MATLAB software. For each image, the data treatment consisted of: (1) background removal by Gaussian filtering and image subtraction, (2) thresholding and binarization of the resulting image, and (3) automatic detection of silica particle boundaries from the binary image using ImageJ software. Thereafter, statistics of particle diameter (taken as Feret's diameter, i.e. the longest distance between any two points along the detected particle boundary) and the 1st nearest neighbour distance (1st NND) were calculated in MATLAB.

3D surface topography analysis was carried out by using a Veeco Wyko® NT1100 optical profiling system in vertical scanning interferometry (VSI) mode from both film sides (147 µm × 96 µm scanning area). The surface topography data was levelled by 2nd order polynomial background subtraction and surface roughness statistics were calculated using the open-source Gwyddion software.

Measurement sequences for thermally stimulated and isothermal current methods

For the TSDC measurement the standard procedure was (unless otherwise specified): (i) polarization at DC field E_p=100 V/µm for 40 min under isothermal conditions at T_p = 80 °C, (ii) rapid cooling to T_0 = −50 °C; hold isothermally for 5 min, (iii) removal of the poling voltage and short-circuiting of the sample through the electrometer; hold isothermally for 3 min, (iv) linear heating at β = 3.0 °C/min heating rate up to $T_{max}\approx$140 °C while recording the depolarization current. For TSPC measurements the heating-cooling-heating sequence was

the same as that used for TSDC measurements, but the electric field was applied during the main thermally stimulated heating phase from −50 °C to 140 °C. For the ICC/IDC measurements the samples were held isothermally at 100 °C and charging current under DC electric field of 100 V/μm was measured for 24 h (volt on), followed by the measurement of discharge current for 6 h (volt off).

Derivation of trapping parameters from PEA space charge profiles

Stored charge density at a specific field and depolarization time, $q(E,t)$, was derived from the space charge profile measurements as:

$$q(E,t) = \frac{1}{L}\int_0^L \left|q_p(E,x,t)\right| dx \tag{1}$$

where 0 and L denote the cathode and anode positions and $q_p(E,x,t)$ is the space charge profile for a given poling field E. The electric field distribution $E(x,t)$ can be evaluated from space charge profile q_p, since:

$$\nabla \cdot E(x,t) = -\frac{q_p}{\varepsilon} \tag{2}$$

where ε is the permittivity of the specimen tested.

An approximated estimation of apparent trap-controlled mobility of charges μ can also be derived from those measurement in time[1]:

$$\mu(E,t) = \frac{\varepsilon}{q^2(t)}\frac{dq(E,t)}{dt} \tag{3}$$

where $dq(E,t)/dt$ is the slope of the depolarization curve at time t, after a polarization period at a medium field E elapsed. Once the apparent trap-controlled mobility is known, the trap depth could be approximated from:

$$W = k_b T \ln\left(\mu \frac{h}{eR^2}\right) \tag{4}$$

where k_b is Boltzmann's constant, T is the temperature, R is the mean distance between localized states (5×10^{-7} m in the calculations of this work), e is the electron charge and h is the Planck's constant.

Non-isothermal crystallization kinetics analysis

According to the Avrami theory, the time-dependent relative degree of crystallinity $X(t)$ is:

$$X(t) = 1 - exp(-Z_t t^n) \tag{5}$$

where Z_t is the cooling rate dependent crystallization rate constant, n is the Avrami exponent, and transformation between time t and temperature T is obtained from $t = (T_0 - T)/\Phi$ where Φ is the cooling rate. Eq. (5) can be rearranged by taking its double logarithm:

$$\log\{-\ln[1 - X(t)]\} = n\log(t) + \log(Z_t) \tag{6}$$

Thus, plotting of $\log\{-\ln(1 - X(t))\}$ vs. $\log(t)$ should yield linear plots where the slope and intercept of the fitted line correspond to n and $\log(Z_t)$, respectively. Further, the crystallization rate constant at unit cooling rate can be obtained from $\log(Z_c) = \log(Z_t)/\Phi$ and the crystallization half-time from $t_{1/2} = \left(\ln(2)/Z_c\right)^{1/n}$.

According to the combined Ozawa–Avrami model:

$$\log(Z_t) + n\log(t) = \log(k(T)) - m\log(\Phi) \tag{7}$$

or

$$\log(\Phi) = \log(F(T)) - b\log(t) \tag{8}$$

where $k(T)$ is a cooling function, n is the Avrami exponent, m is the Ozawa exponent and b is the ratio n/m. The function $F(T) = [k(T)/Z_t]^{1/m}$ is a kinetic parameter referring to the value of cooling rate needed to reach a defined degree of crystallinity at unit crystallization time, thus having a well-defined physical meaning. According to Eq. (8), at a given degree of crystallinity a plot of $\log(\Phi)$ against $\log(t)$ should yield a straight line fit with the intercept and slope corresponding to $\log(F(T))$ and $-b$, respectively.

Cast film DSC data

Table S1 presents the parameters from the cast film heating–cooling–heating data DSC tests (10 °C/min). Table S2 presents the parameters from the non-isothermal DSC crystallization kinetics tests on cast films (varying cooling rates of 2.5, 5, 10 and 20 °C/min).

Table S1. Cast film DSC heating–cooling–heating data.

Material	Silica (wt-%)	φ (wt-%)	1st heating ΔH_f (J/g)	1st heating X_{DSC} (%)	1st heating T_{om} (°C)	1st heating $T_m(\alpha)$ (°C)	1st cooling T_c (°C)	2nd heating T_g (°C)	2nd heating ΔH_f (J/g)	2nd heating X_{DSC} (%)	2nd heating T_{om} (°C)	2nd heating $T_m(\alpha)$ (°C)
PP-0-HighAO	0.0	–	92.2	54.0	150.1	162.8	117.1	−6.2	100.9	59.2	155.0	159.2
PP-1.0-HighAO	1.0	0.82	91.4	53.6	150.6	162.7	118.7	−6.7	101.2	59.3	155.6	159.7
PP-2.0-HighAO	2.0	1.45	90.5	53.1	150.6	162.7	119.3	−4.7	100.2	58.6	155.8	160.0
PP-4.5-HighAO	4.5	2.85	88.1	51.8	151.2	162.6	119.2	−6.6	98.6	58.1	155.7	160.0

Table S2. Non-isothermal DSC crystallization parameters.

Material	Silica (wt-%)	Avrami parameters	Cooling rate, Φ (°C/min) 2.5	5	10	20	Combined Avrami and Ozawa analysis X (%)	20 %	40 %	60 %	80 %
PP-0-HighAO	0.0	T_c (°C)	121.5	119.2	116.9	114.3	b	1.13	1.15	1.17	1.20
		ΔH_c (J/g)	98.2	96.5	95.4	93.5	ln $F(T)$	1.55	1.75	1.89	2.05
		n	4.46	4.21	4.17	4.23					
		Z_c	0.20	0.79	1.15	1.21					
		$t_{1/2}$ (min)	1.32	0.97	0.88	0.88					
PP-1.0-HighAO	1.0	T_c (°C)	123.4	120.7	117.9	114.7	b	1.08	1.09	1.10	1.13
		ΔH_c (J/g)	94.8	93.5	90.5	89.1	ln $F(T)$	1.75	1.94	2.08	2.23
		n	4.23	4.06	4.17	4.25					
		Z_c	0.15	0.70	1.08	1.18					
		$t_{1/2}$ (min)	1.44	1.00	0.90	0.88					
PP-2.0-HighAO	2.0	T_c (°C)	124.1	121.3	118.3	115.1	b	1.06	1.07	1.08	1.11
		ΔH_c (J/g)	94.7	92.4	89.8	87.9	ln $F(T)$	1.77	1.96	2.10	2.25
		n	4.51	4.03	4.05	4.16					
		Z_c	0.12	0.69	1.07	1.17					
		$t_{1/2}$ (min)	1.47	1.00	0.90	0.88					
PP-4.5-HighAO	4.5	T_c (°C)	124.2	121.6	118.6	115.6	b	1.07	1.08	1.09	1.11
		ΔH_c (J/g)	93.8	92.4	90.0	89.3	ln $F(T)$	1.78	1.96	2.10	2.25
		n	4.36	4.28	4.12	4.26					
		Z_c	0.14	0.66	1.08	1.18					
		$t_{1/2}$ (min)	1.45	1.01	0.90	0.88					

Polarized optical microscopy on cast and BOPP film sections

Figure S1 presents cross-sectional POM images of cast and BOPP film sections.

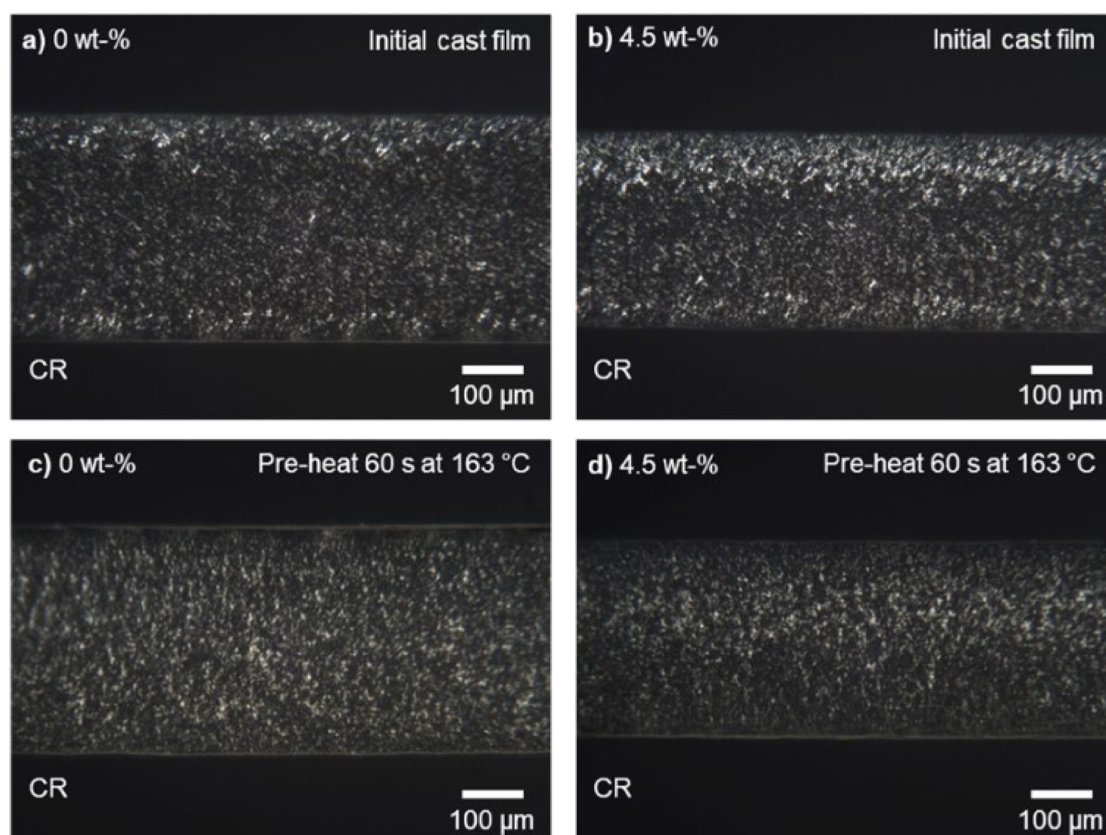

Figure S1. Exemplifying cross-sectional OM micrographs of **a)** 0 wt-% and **b)** 4.5 wt-% PP-silica cast films under cross-polarized reflected light (top row). The POM images in **c)** and **d)** present the corresponding cast film morphologies after 60 s of annealing at 163 °C (just before biaxial stretching). CR denotes chill roll side.

Effect of voids, biaxial stretching temperature and stretch ratio on the TSDC spectra and DC dielectric strength of silica-BOPP films

As detailed elsewhere [2], the biaxial-stretching induced morphological changes were also studied in detail with selected silica-BOPP films. In brief, both increasing biaxial stretching ratio and temperature were found to increase the high temperature TSDC peak intensity (T_p around 100 °C), hence implying an increase in deep trap density with the above factors. Considering the increasing biaxial stretch ratio, the above effect can be attributed with a modification of crystallinity, crystallite size and crystallite orientation [3], as these properties affect the quantity of charge trap sites at the amorphous–crystalline boundaries [4,5]. The (asymmetrical) thickness-directional film morphology "gradient" [6] and surface texture characteristics of the biaxially stretched film likely play a significant role here [7]. On the other hand, the increase of deep trap density with increasing pre-heating/stretching temperature is somewhat unexpected, as the films biaxially stretched at lower temperatures

exhibited relatively large amount of voids (see Figure 6) and were thus expected to show higher charge trapping propensity, as is typically observed for voided/cellular iPP films [8]. It is thus likely that the quantity and dimensions of the voids even at 155 °C were not large enough to have a significant effect on charge trapping, and hence the observed increase in deep trap density with increasing pre-heating/stretching temperature is mostly associated with other morphological changes [3].

The effects of biaxial stretch ratio and pre-heating/stretching temperature on the room temperature large-area DC dielectric breakdown characteristics of 4.5 wt-% silica-BOPP film have been presented separately in ref. [2]. An increase in breakdown strength (Weibull α) was observed with an increasing stretch ratio from 3.5 × 3.5 up to 6.0 × 6.0, along with an increasing trend also observed for Weibull β. The increase in dielectric strength with biaxial (area) stretching ratio can be attributed to increased chain orientation and formation of fibrillar BOPP morphology as discussed elsewhere [7], and may also be related with formation of higher density morphology-related charge traps. On the other hand, while increasing biaxial stretching temperature also resulted in a slight increase in dielectric strength (Weibull α), a significant reduction in Weibull β was concurrently observed. Thus, biaxial stretching very close to the melting point of the polymer likely resulted in partial melting and poor orientation of the polymer chains, hence resulting in decreased breakdown performance even though the voids and cavities, which in principle may affect the dielectric strength [9,10], were eliminated (compare with the OM analysis presented in Figure 6). Lastly, no clear correlation between film surface roughness and dielectric strength could be obtained, indicating that, as opposed to agglomerates, silica-BOPP film surface structure may be a less significant factor for the dielectric strength.

Lastly, considering the agglomerates and voids within the biaxially stretched films, the typical height of the void region or the typical dimension of the agglomerates are significantly lower in proportion to the total film thickness. Thus, during breakdown strength measurement, the electric field (in film thickness direction during) will re-distribute mostly to the intact PP volume. It is well known that PP has a high DC breakdown strength, and even despite such voids or defects the film can withstand substantially high electric stress before breakdown. As an extreme example, consider e.g. cellular electret PP films as presented by Qiu et al. [9] with high porous/void fraction (40—140 µm thickness): even in such a case the PP film can withstand 200-300 V/µm which is on par with bulk PP reference insulation in similar thickness range (note that for the BOPP films studied in the present manuscript, the film thickness is much lower, 5–10 µm, and the films are biaxially stretched, leading to as high breakdown strength as ~700 V/µm).

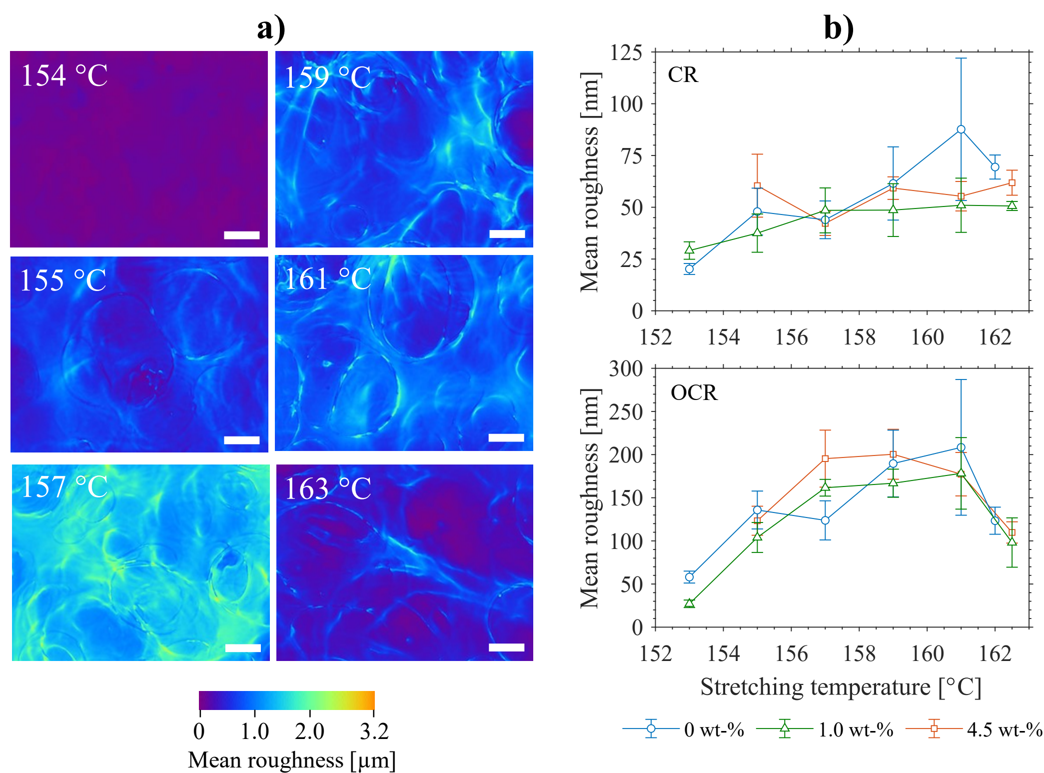

Figure S2. a) 3D optical profilometer surface height profiles of 4.5 wt-% silica-BOPP films produced at various biaxial stretching temperatures (PP-4.5-HighAO, stretch ratio 6.0 × 6.0). The scale bar is 100 µm. **b)** Mean (area) surface roughness of 0–4.5 wt-% silica-BOPP films as a function of stretching temperature for the chill-roll side (CR) and opposite side of chill-roll (OCR), respectively. The error bars denote standard deviation.

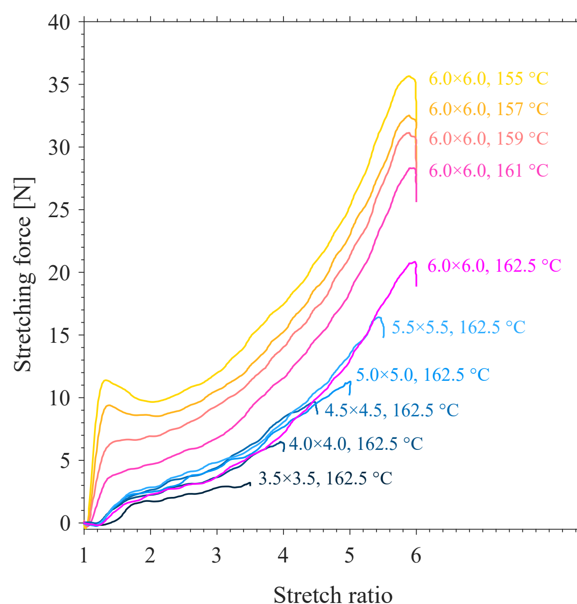

Figure S3. Force vs. stretch ratio at different stretch temperatures and elongations (PP-4.5-HighAO). For clarity, only MD-directional forces are shown (TD forces are similar under equibiaxial stretching).

SEM/EDS analysis of silica agglomerate

SEM/EDS analysis of non-oriented and biaxially-oriented cast films was carried out to investigate the nature of the particles/agglomerates. For silica agglomerates, such as the one imaged with SEM in Figure 3b (clearly seen to consist of agglomerated silica aggregates and primary particles), a clear indication of elemental Si and O was confirmed by the EDS analysis (see the additional figure below). However, it is important to remark that the sample preparation and analysis by SEM/EDS is not straightforward for very thin films and most importantly the statistical significance of the analysis is, in our view, not satisfactory. Moreover, considering the melt-blending approach via twin screw extruder—despite meticulous cleaning and preparation before compounding as in our study—there always exists a small possibility of some kind of cross-contamination or release of residual degraded (or "burned") polymer particles from preceding processing trials. This is also widely acknowledged fact in the plastics processing industry.

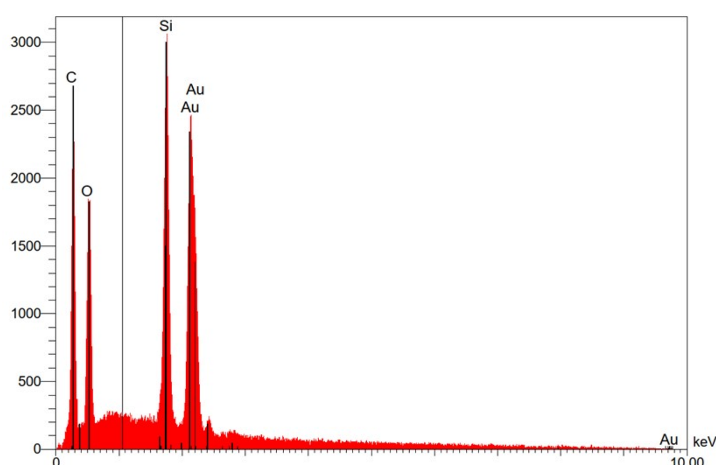

Figure S4. SEM/EDS analysis of a silica agglomerate seen in 4.5 wt-% silica-PP nanocompound. The sample was sputter coated with Au.

References

[1] G. Mazzanti, G.C. Montanari, J.M. Alison, A space-charge based method for the estimation of apparent mobility and trap depth as markers for insulation degradation-theoretical basis and experimental validation, IEEE Trans. Dielectr. Electr. Insul. 10 (2003) 187–197. doi:10.1109/TDEI.2003.1194099.

[2] I. Rytöluoto, M. Niittymäki, K. Lahti, E. Saarimäki, T. Flyktman, M. Paajanen, M. Karttunen, Silica-Polypropylene Nanocomposites for Film Capacitors: Structure–Property Studies and the Role of Biaxial Stretching Conditions, Proc. Nord. Insul. Symp. (2019) 123–128. doi:10.5324/nordis.v0i26.3291.

[3] L. Capt, Simultaneous biaxial stretching of isotactic polypropylene films in the partly molten state, McGill University, 2003. http://digitool.library.mcgill.ca:80/R/-?func=dbin-jump-full&object_id=82839&silo_library=GEN01.

[4] K. Yahagi, Dielectric Properties and Morphology in Polyethylene, IEEE Trans. Electr. Insul. EI-15 (1980) 241–250. doi:10.1109/TEI.1980.298316.

[5] J.K. Nelson, Breakdown Strength of Solids, in: R. Bartnikas, R. Eichhorn (Eds.), Eng. Dielectr. Vol. IIA Electr. Prop. Solid Insul. Mater. Mol. Struct. Electr. Behav., ASTM International, Philadelphia, 1983: pp. 445–520. doi:10.1520/STP37840S.

[6] A. Thielen, J. Niezette, G. Feyder, J. Vanderschueren, Thermally stimulated current study of space charge formation and contact effects in metal-polyethylene terephthalate film-metal systems. I. Generalities and theoretical model, J. Phys. Chem. Solids. 57 (1996) 1567–1580. doi:10.1016/0022-3697(96)00062-5.

[7] I. Rytöluoto, A. Gitsas, S. Pasanen, K. Lahti, Effect of film structure and morphology on the dielectric breakdown characteristics of cast and biaxially oriented polypropylene films, Eur. Polym. J. 95 (2017). doi:10.1016/j.eurpolymj.2017.08.051.

[8] J. Hillenbrand, N. Behrendt, V. Altstädt, H.-W. Schmidt, G.M. Sessler, Electret properties of biaxially stretched polypropylene films containing various additives, J. Phys. D. Appl. Phys. 39 (2006) 535–540. doi:10.1088/0022-3727/39/3/017.

[9] X. Qiu, F. Groth, W. Wirges, R. Gerhard, Cellular polypropylene foam films as DC voltage insulation and as piezoelectrets — A comparison, IEEE Trans. Dielectr. Electr. Insul. 25 (2018) 829–834. doi:10.1109/TDEI.2018.007192.

[10] E. Ildstad, T. Haave, Conduction and partial discharge activity in HVDC cable insulation of lapped polypropylene films, in: ICSD'01. Proc. 20001 IEEE 7th Int. Conf. Solid Dielectr. (Cat. No.01CH37117), IEEE, 2001: pp. 137–140. doi:10.1109/ICSD.2001.955542.